Two-dimensional Si crystal growth during thermal annealing of Au/polycrystalline-Si bilayers

L. H. Allen, J. R. Phillips, D. Theodore, C. B. Carter, R. Soave, and J. W. Mayer
Department of Materials Science and Engineering, Cornell University, Ithaca, New York 14853

G. Ottaviani
Department of Physics, University of Modena, via Campi 213/A, I-41100 Modena, Italy
(Received 23 June 1989; revised manuscript received 13 September 1989)

Interactions between Au and polysilicon (where polysilicon denotes polycrystalline Si) thin films during thermal annealing at temperatures below 300 °C produce large-grain Si crystals (*c*-Si). Si is transported from the fine-grain polysilicon laterally through the Au layer to form large (400-μm^2) plate-like-shaped single crystals of Si of thickness equal to that of the Au layer. The Si crystals displace the Au in the original Au layer and at the same time the Au penetrates into the polysilicon. X-ray diffraction data indicate that the Si crystals have the same preferred orientation $(1\bar{1}0)$ as the initial polysilicon film. The driving force for this transformation is the reduction of the interface energy at the grain boundaries of the polysilicon. It is concluded that the large grains from the polysilicon layer grow at the expense of the smaller grains.

I. INTRODUCTION

The reaction between Au and polysilicon (where polysilicon denotes polycrystalline Si) is related to two topics of interest. The first area relates to the stability of metal/Si interfaces, which is associated with reliability issues in electronic devices. The second area of interest is the growth of Si crystals in the solid phase,[1,2] which is related to work on Si lateral solid-phase-epitaxy growth, currently being investigated for possible applications in three-dimensional integrated circuits.[3] There are two general classes of metals in metal/polysilicon systems:[4,5] those metals which form stable silicide phases (e.g., WSi_2, $MoSi_2$, PtSi, etc.) and those which form eutectics with Si including Au (360 °C), Ag (830 °C), and Al (577 °C). Reactions in the eutectic systems result in the formation of large-grained Si.[6-8]

Most work involving thermal reactions in the Si eutectic systems has been done on the Al/polysilicon system.[9] Experiments[10-12] have demonstrated the growth of Si crystallites during thermal anneals of Al and polysilicon over a wide range of Al/Si thicknesses. The Al/Si system was also used[13-15] to epitaxially grow Si onto a Si substrate using a layer configuration of amorphous Si/Al/Si substrate.

This study investigates the structure of the Si crystallites formed during thermal annealing of Au/polysilicon bilayers, where the thickness of the Au layer is less than the polysilicon layer. This reaction[16,17] produces large-grained Si crystals (*c*-Si), as was found in the Al/Si system. The unique characteristic of the Au/Si system is that the grain growth of Si occurs at relatively low temperatures ($\approx$300 °C) as compared to the typical crystallization temperature of amorphous Si ($\approx$500–600 °C).[1] We focus the analysis on Si by characterizing the location, size, shape, and orientation of the crystals. Analyses include x-ray diffraction (XRD), scanning electron microscopy (SEM), and planar and cross-sectional transmission electron microscopy (TEM).

This paper deals with the end state of the reaction, describing the process in terms of the redistribution and other time-independent characteristics of the components: Au, polysilicon, and c-Si. The accompanying paper investigates the time and temperature effect on crystal growth and discusses the rate-limiting processes that control the kinetics of the reaction.[18]

II. SAMPLE PREPARATION

Au/polysilicon bilayers were fabricated on inert substrates including quartz wafers and thermally oxidized single-crystal Si substrates. Polysilicon was deposited by the low-pressure chemical-vapor-deposition (LPCVD) process at 620 °C to a thickness of 100–400 nm. The polysilicon thin films had columnar grain structure, which is typical for films grown with LPCVD at this temperature.[19] After cleaning the surface of the polysilicon with a buffered hydrofluoric-acid solution, Au was thermally evaporated onto the polysilicon thin films at a pressure of 5×10^{-6} Torr to a thickness of 80–250 nm.

Samples fabricated on quartz substrates were used in obtaining XRD data since diffraction from this substrate would not interfere with the XRD intensities generated by the polysilicon and c-Si thin films. Samples needed for planar TEM investigations were made by first removing the polysilicon from the SiO_2/Si substrate prior to Au deposition. This was done by lifting off the polysilicon by using a concentrated hydrofluoric-acid solution. Cross-sectional TEM analyses were made on the Au/polysilicon layers that were deposited on thermally oxidized Si substrates.

III. RESULTS

A. Si crystal growth during thermal annealing

The Au/polysilicon bilayers were annealed in a vacuum system maintained at a nominal pressure of 1×10^{-7}

 ©1990 The American Physical Society

Torr at 270 °C. The appearance of Si crystal was easily observable via SEM imaging using a JEOL™ 35 system. SEM micrographs of a partially annealed sample are shown in Fig. 1. The Si crystals appear as faceted dark patches; the contrast is due to the two different elements at the surface (Au and Si). The area of each crystal depends on the duration of the anneal, but eventually they impinge on one another, displacing the entire original Au layer, leaving the top layer as a "patchwork-quilt" network of crystal Si plates.

A cross-sectional TEM micrograph of a partially annealed sample is shown in Fig. 2. The initial thickness of the Au was 170 nm and the polysilicon was 400 nm thick. The Au appears as the dark areas in the TEM micrograph. The Si crystal, shown in the micrograph, has the shape of a flat plate having a thickness equal to the original Au layer and is supported from below by the underlying polysilicon layer. During the anneal the Au/(*c*-Si) interface at the edge of the crystal moves laterally in the direction of the Au layer; the velocity of this interface determines the growth rate of the crystal. There are no observable inclusions of Au within the crystal.

During the growth of the Si crystals the Au redistributes by vertically penetrating the polysilicon layer and accumulating at the bottom of the polysilicon layer. Accumulation of Au at the bottom polysilicon/SiO_2 interface is expected since the Si at this interface is more disordered (smaller grains) and should dissolve more easily into the Au as compared to the subsequent layers of Si that eventually form larger columnar grains. The three-dimensional distribution of the Au after annealing was directly observed by etching the entire sample in a hydrofluoric- and nitric-acid solution. This solution dissolved the Si and SiO_2 releasing the Au from the substrate as an isolated, free-standing completely intact Au film, which was then analyzed via SEM. The Au and Si

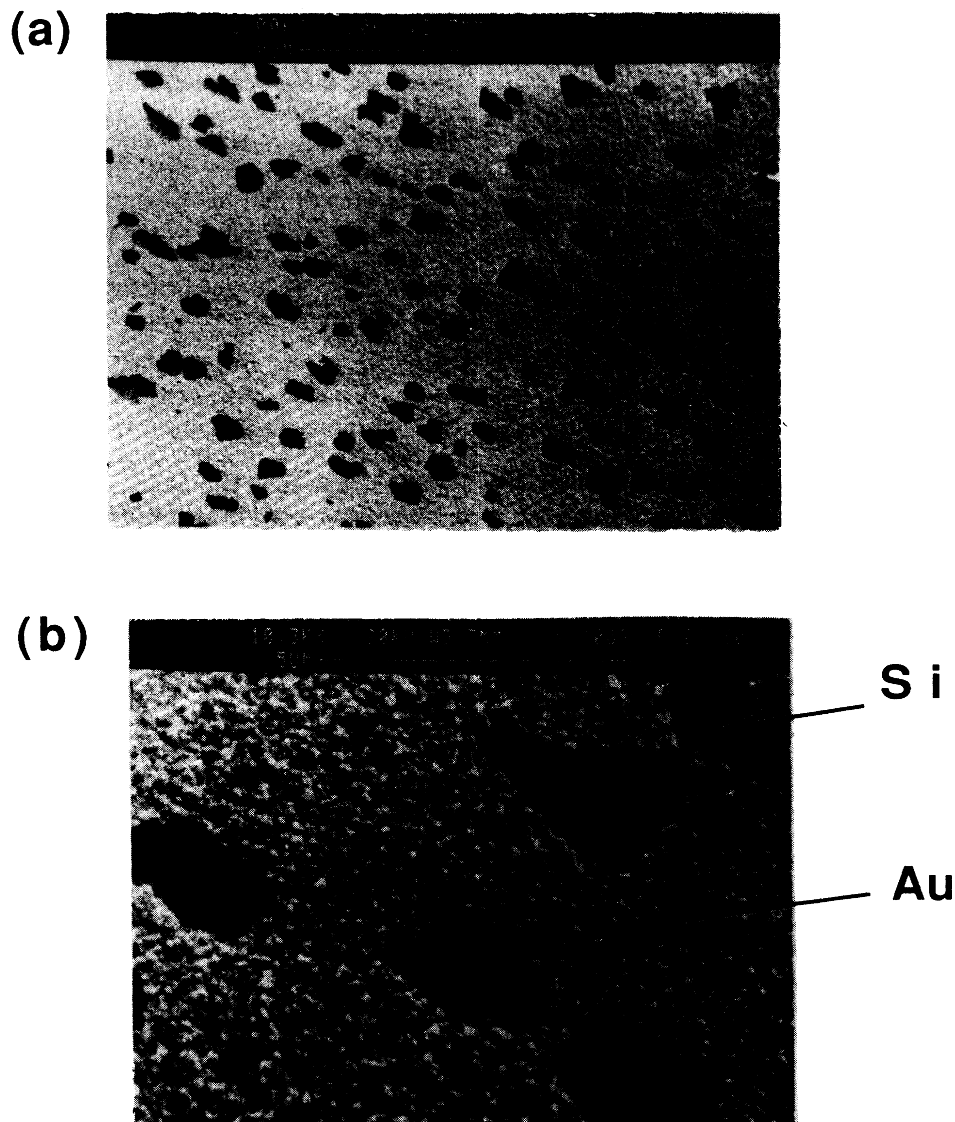

FIG. 1. SEM photograph of Au($\approx$170 nm)/polysilicon($\approx$400 nm)/SiO_2 after 270-°C vacuum-furnace annealing for 240 min.

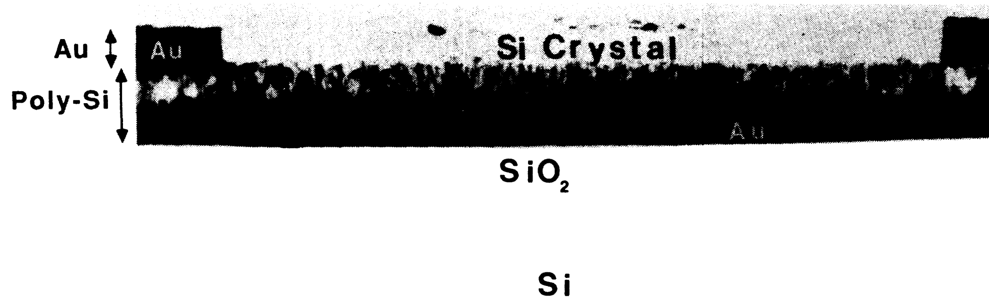

FIG. 2. Cross-sectional TEM data of Au($\approx$200 nm)/polysilicon($\approx$400 nm)/SiO_2 sample after 250-°C vacuum-furnace annealing.

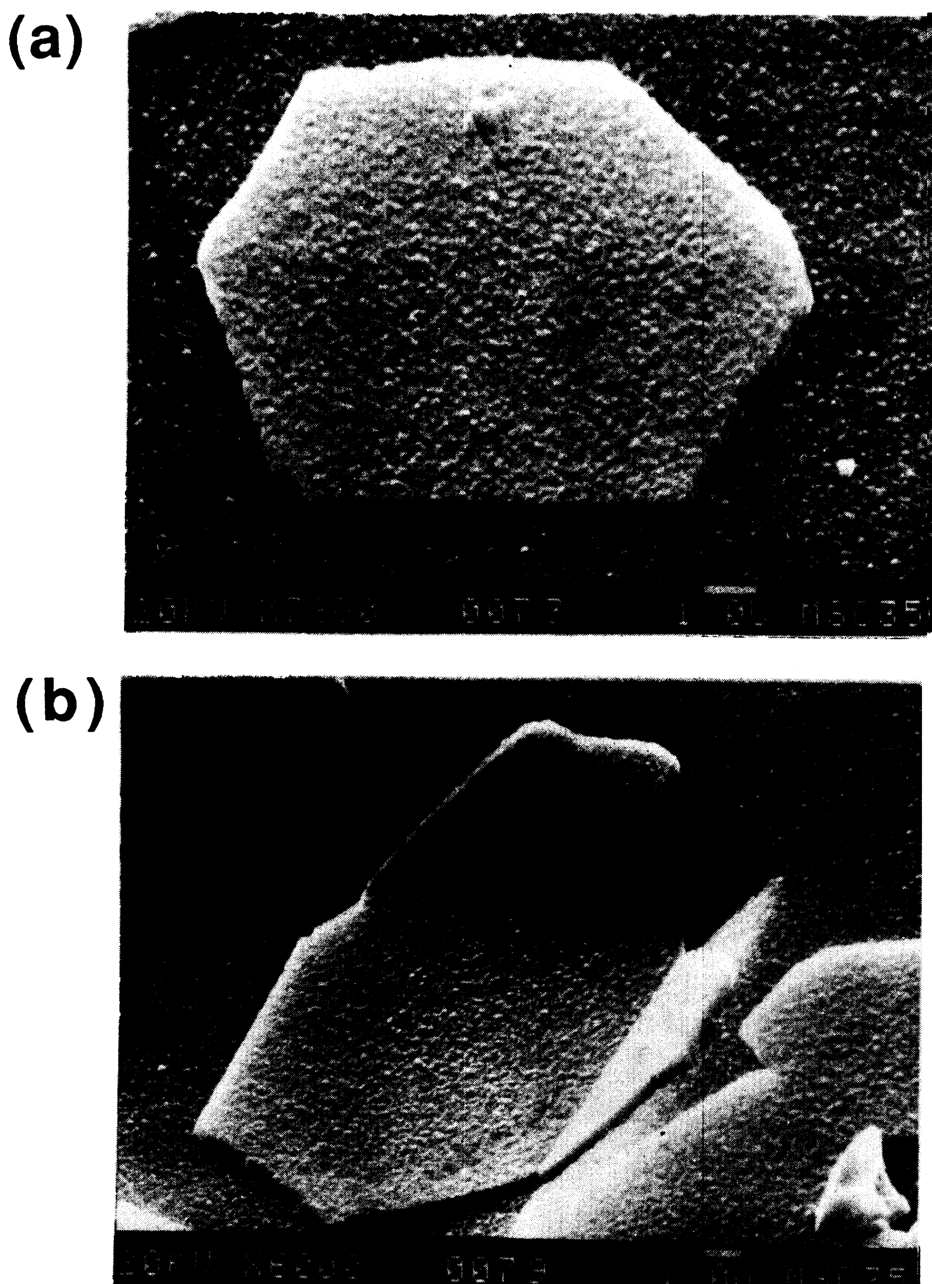

FIG. 3. SEM micrograph of Si crystals on polysilicon after Au was selectively etched. Au($\approx$250 nm)/polysilicon($\approx$400 nm)/SiO_2 samples were fabricated on (a) flat and (b) stepped-surface substrates.

displace each other in such a way as to keep the entire thickness of the composite layer constrained to the original geometry of the sample. No voids or "hillock" formation were observed.

The Si crystal plates can also be observed in planar view via SEM by removing the Au layer using a potassium iodide (KI) solution. The crystal shown in Fig. 3(a) was grown with Au/polysilicon bilayers deposited onto a flat substrate. The crystal shown in Fig. 3(b) was prepared on a substrate that had a stepped surface, and it demonstrates that the shape of the crystals follows the contour of the original Au/polysilicon bilayer deposited across the step.

Preliminary cross-sectional TEM investigation of this type of obtuse crystal indicates that it is one complete crystal. Apparently, the lateral growth of the crystals is not restricted to flat surfaces.

This conformal crystal-growth process may provide possibilities for growing single crystals of unusual shapes.

Si crystal growth was also observed by TEM during *in situ* annealing. The redistribution of the Au during the annealing allowed the Si crystals to be seen via bright-field (BF) imaging. Two samples, with different Au thicknesses, were made. As expected, the sample with the thicker (200 nm) Au layer produced thicker Si crystals [Fig. 4(a)], as is evident from the presence of Kikuchi patterns [Fig. 4(b)]. This is compared to the diffraction pattern of the thin Si crystals [Fig. 4(c)] formed with a thinner (80 nm) Au layer which shows a diffraction-spot pattern [Fig. 4(d)].

The redistribution of the Si was also analyzed on annealed samples which had the Au chemically removed using a KI solution. A TEM planar-view micrograph [Fig. 8(c)] shows three distinct regions in the vicinity of a crystal. The first region is the polysilicon area far away from the crystal. The selected-area-diffraction (SAD) pattern of this area, shown in Fig. 5(a), is similar to the SAD pattern obtained from the original unreacted polysilicon layer, indicating minor, if any, change in the polysilicon layer in this area. The second region is the crystal area. The SAD data taken from this area with an aperture much smaller than the crystal are shown in Fig. 5(b), con-

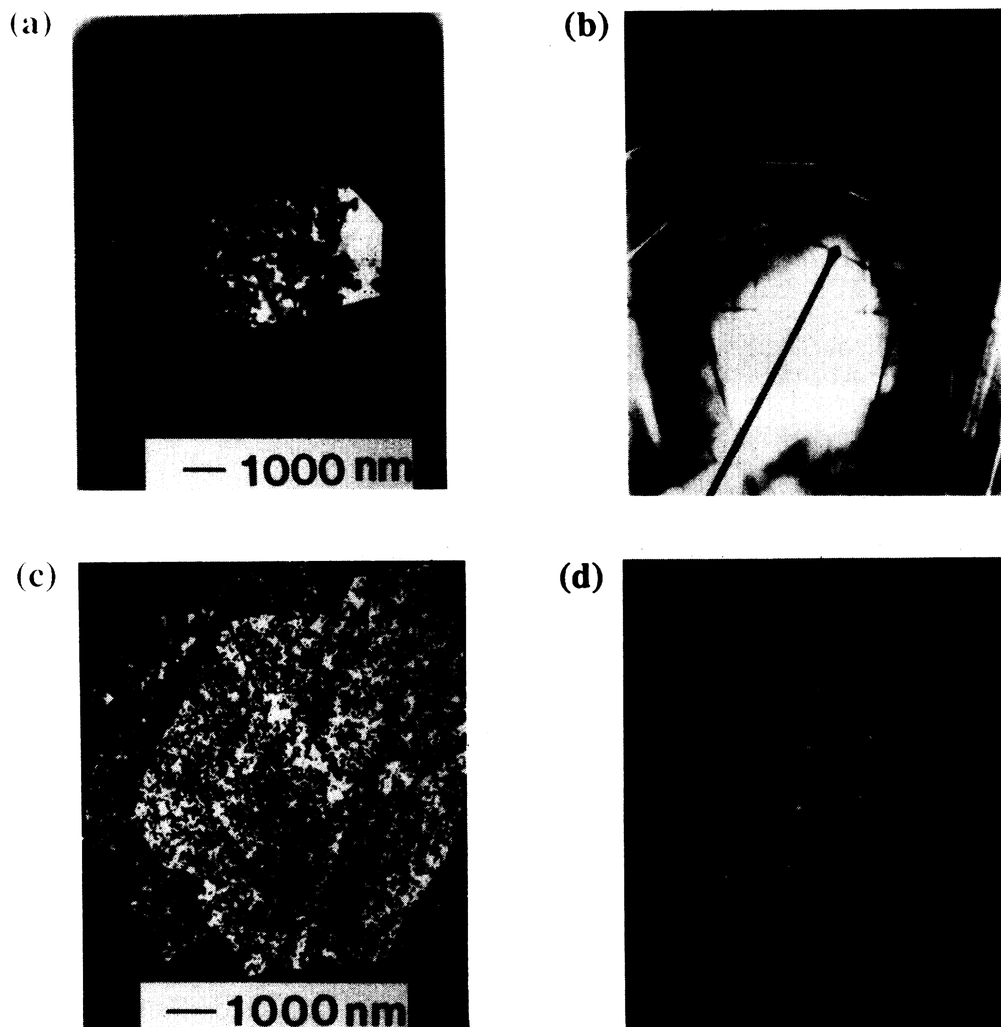

FIG. 4. BF image and diffraction micrographs of (a) and (b) thick and (c) and (d) thin Si crystals. The samples were made with thick [(a) and (b)] (200 nm) and thin [(c) and (d)] layers of Au on Si(100 nm). The Au/polysilicon samples were annealed (250–300 °C) *in situ* in TEM.

sisting of Debye rings generated by the polysilicon superimposed on a Kikuchi pattern generated by the Si crystal. Both Kikuchi and Debye-ring diffraction patterns appear together because both the crystal and the underlying bed of polysilicon diffract the electron beam. Because of the size of the aperture, only the polysilicon under the crystal will diffract the beam. The third region is the area laterally adjacent to the crystal. The variation of the BF intensity near the edge of the crystal, shown in Fig. 5(c), qualitatively indicates the extent and lateral range of Si depletion from the polysilicon film due to the lateral transport of Si from the polysilicon layer to the crystal. The Si that makes up the crystal was transported over distances of several micrometers.

The Si crystals grown from the Au/polysilicon bilayers did have crystalline imperfections. Bright-field [Fig. 6(a)] and dark-field (DF) [Fig. 6(b)] images of an annealed sample, after the Au was removed, indicate the presence of defects (e.g., twins) in a thin (100 nm) Si crystal.

Throughout this investigation no metastable phases of Au-Si were identified. The major phases present via TEM and XRD evaluations were Au and Si.

B. Orientation of the Si crystals

The Au/polysilicon reaction was also analyzed with XRD using a SCINTAG™ diffractometer. Analysis was complicated by the condition that both the Si crystals and the polysilicon had preferred orientation. Consequently, the relative tilt of the sample during XRD experiments is important when comparing different samples and different peak intensities. One particular method which analyzes peak intensity as a function of sample orientation is the pole-figure method.[20] This method maps the intensity of a given set of $\{hkl\}$ poles as function of the orientation (tilt ψ and rotation ω) of the sample.

Pole-figure data were taken with the Si 220 reflection on unannealed samples and showed that the distribution of the $\{110\}$ poles was not random but concentrated at zero tilt ($\psi=0°$), indicating that the grains had a (110) preferred orientation. This result was expected since polysilicon films grown at 620 °C typically have (110) preferred orientation.[19] The same pole-figure routine was applied to annealed samples and showed that the new

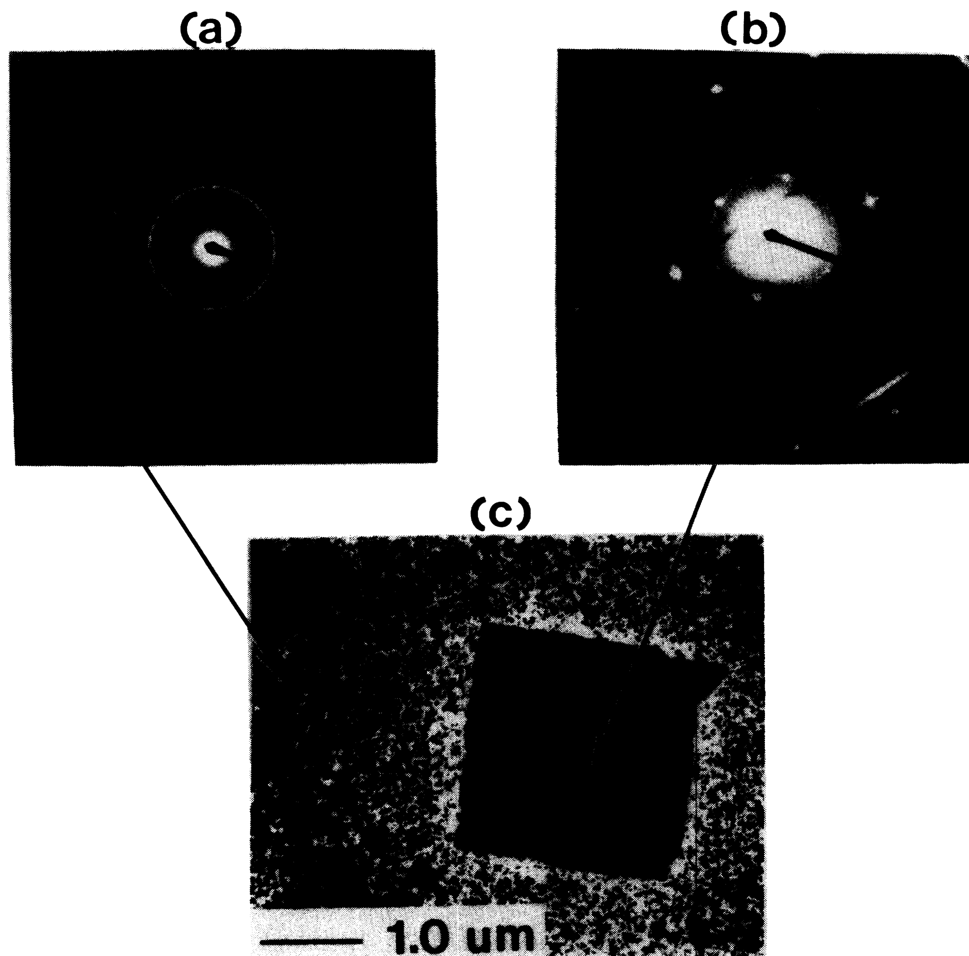

FIG. 5. Planar TEM data of Au(200 nm)/polysilicon(100 nm) *in situ* annealed sample after Au was etched, showing Si depletion in area adjacent to crystal: (a) Debye rings from the polysilicon, and (b) Kikuchi pattern and Debye rings from the crystal and polysilicon, and BF micrograph.

crystals have the same (110) orientation as the as-deposited sample. The intensity of the 220 reflection is highest at zero tilt ($\psi=0°$), as shown in Fig. 7(a), with the majority of the grains aligned to within 13° ($\Delta\Psi \approx 13°$) of the normal to the surface. The pole-figure method was also applied to the annealed samples using the Si(111) reflection, and the distribution of intensity is shown in Fig. 7(b).

The maximum intensity for the (111) reflection occurs when the sample is tilted ($\psi \approx 30°-40°$) off normal, which again confirms the (110) preferred orientation since the (110) and (111) poles in the crystal are separated by an angle of 35.3°. The uniformity of the intensity versus rotated angle ω indicates that the Si plate crystals are randomly oriented about the (110) pole, indicating [110] fiber texture.

The (110) preferred orientation of annealed samples was confirmed qualitatively with TEM by a random inspection of crystals. The (110) diffraction pattern was the most frequently obtained pattern when the sample tilt was restricted to a limited range about the sample normal. The BF image [Fig. 8(a)] and diffraction pattern [Fig. 8(b)] were obtained from one particular (110)-oriented crystal, where the sample was tilted $\approx 11°$ off the sample normal. The same (110) diffraction pattern was obtained at all tested locations of this crystal without additional changes in tilt, which confirms that the crystal is indeed a single crystal. The features in the micrograph in the area framed by the crystal are not due to the crystal, which is essentially transparent, but are due to the material beneath the crystal: the remaining polysilicon and Au which has penetrated the polysilicon film. There were crystals which did not have the (110) orientation, but they were the exceptions.

Although the orientation of the unannealed and annealed samples were similar, there were two significant differences in the XRD data between the annealed and unannealed samples: an increase of XRD intensity (increase) and a small shift (decrease) in the 2θ position of the 220 reflection. The increase of peak intensity [Figs.

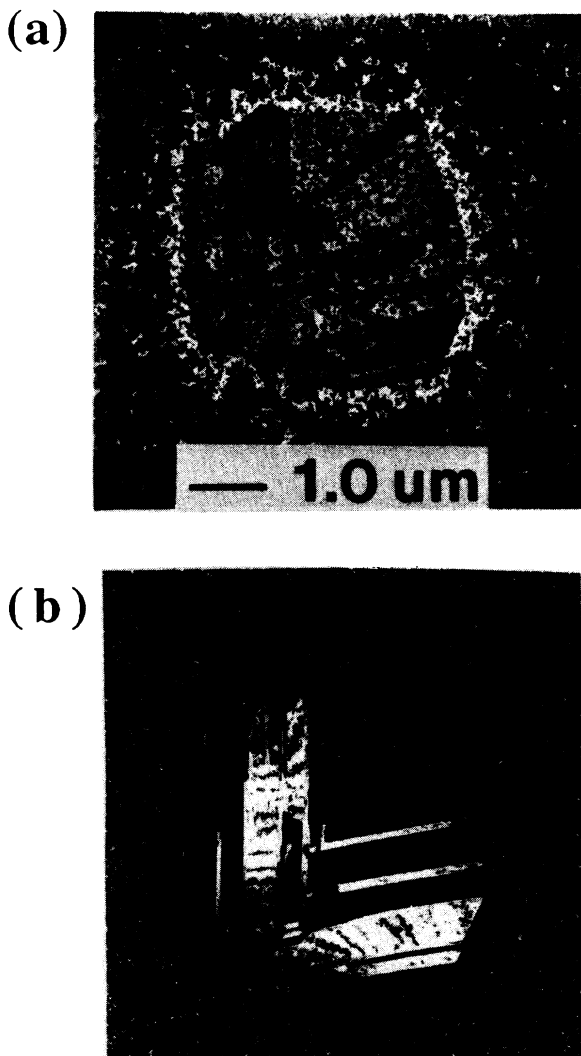

FIG. 6. (a) BF and (b) DF TEM micrographs of Si and polysilicon after Au selective etch. The Au(≈ 100 nm)/polysilicon(≈ 100 nm) samples were annealed *in situ* with TEM.

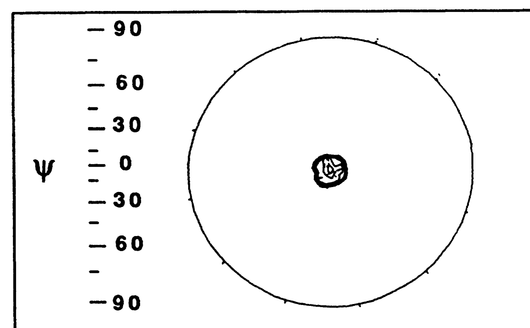

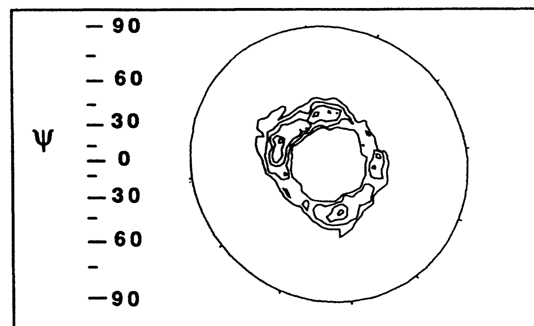

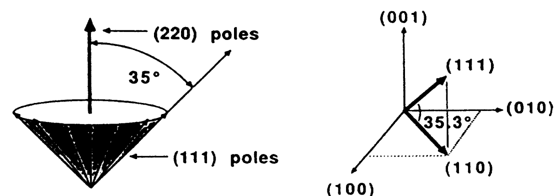

FIG. 7. (220) and (111) pole-figure data showing [110] fiber texture of the annealed Au(≈ 200 nm)/polysilicon(400 nm) sample. The {220} poles are concentrated near the vertical, $\psi=0°$ and the {111} poles concentrated at an off-axis tilt angle ($\psi \approx 30°-40°$).

9(b) and 9(c)] is attributed to the increase size of the Si crystal during annealing. The decrease in the 2θ ($\Delta 2\theta \approx 0.12°$) position of the 220 reflection was observed [Fig. 9(b)] when unannealed and annealed samples were compared. All XRD data were taken with a collimated beam to ensure reproducible sample areas. To reduce other measurement errors, the raw data were corrected for the $K\alpha_1$ and $K\alpha_2$ doublet convolution and adjusted to obtain absolute peak position by using the Au(111) reflection generated by the Au in the sample (an internal reference source). Additional confirmation of changes in peak position were obtained from XRD data collected from a partially annealed sample which shows [Fig. 9(d)] two resolvable (220) Si peaks ($\Delta 2\theta \approx 0.08°$). Assuming that the instrumentation effects have been eliminated, the peak shifts are then attributed to a change in the Si crystal lattice parameter(s).

IV. DISCUSSION

Large, two-dimensional, platelike Si crystals are formed from fine-grained polysilicon when bilayers of Au/polysilicon films are thermally annealed. The discussion focuses on the thermodynamic factors in the system which drive the reaction and the origin of the large crystals.

In discussing the thermodynamic factors, we begin by noting that the main result of the reaction is the increase (by a factor of $\approx 10\,000$) of the size of the Si grains. The composition of the starting reactants and the final products are the same: Si crystals. Therefore, the thermodynamic factors of the reaction must center on a discussion of the microstructure of the initial polysilicon film.

The CVD (620 °C) method forms crystals under extremely nonequilibrium conditions. The free energy of these films is higher than that of a single crystal because of the internal interfaces (grain boundaries, twins, etc.) present in the initial polysilicon layer. This difference in free energy is quantified by modeling the polysilicon film as a mosaic of small crystals (300 Å diameter) interfaced with one another at large-angle twist-tilt grain boundaries. The internal interface energy σ_i at a large-angle grain boundary can be estimated, given a value for the surface energy of $\sigma_s \approx 1$ J/m^2 for Si, by using the relationship[21] $\sigma_i \approx \frac{1}{3}\sigma_s$. From this calculation, we estimate the normalized (over all atoms in the film) free-energy difference due to the internal interface energy to be of the order of ≈ 0.1 eV/atom. We believe that this difference in free energy is responsible for the overall recrystallization process.

Recrystallization does not readily occur in the as-deposited polysilicon films when annealed at temperatures below 1000 °C. In contrast, when Au is deposited on the polysilicon surface, recrystallization occurs at temperatures as low as 200 °C. The difference is due to the kinetic factors in the bilayer system, where the Au layer provides a fast-diffusion path for the transport of Si.

We have shown that the crystal growth proceeds via the lateral transport of Si through the Au. Consequently, there must be differences in the chemical potential μ_{Si} of the Si from place to place (laterally) across the film. This gradient $\nabla\mu_{Si}$ is believed to be present in the as-deposited film and occurs because of physical differences (shapes) between the crystals, which are exposed to Au at the Au/polysilicon interface. There is a wide variation[19] in the size of crystals that form the polysilicon layer. Assuming that smaller crystals have a larger surface curvature than the larger crystals, it can be deduced from the Thomson-Freundlick[21] relationship that the chemical potential of the Si at the small-grained crystal surface should be higher than for the larger-grained Si. This reaction then can be viewed as a form of Ostwald ripening. The Si concentration in the Au will be higher near the small-grained (high-curvature) crystals as compared to the large-grained (lower-curvature) crystals. The small-grained crystals will dissolve and the large-grained crystals will grow.

The final topic of this discussion deals with the initial stages of the reaction and analyzes the origin of the growing crystals. Although it would seem possible for nucleation of Si to occur since there are areas of local super-

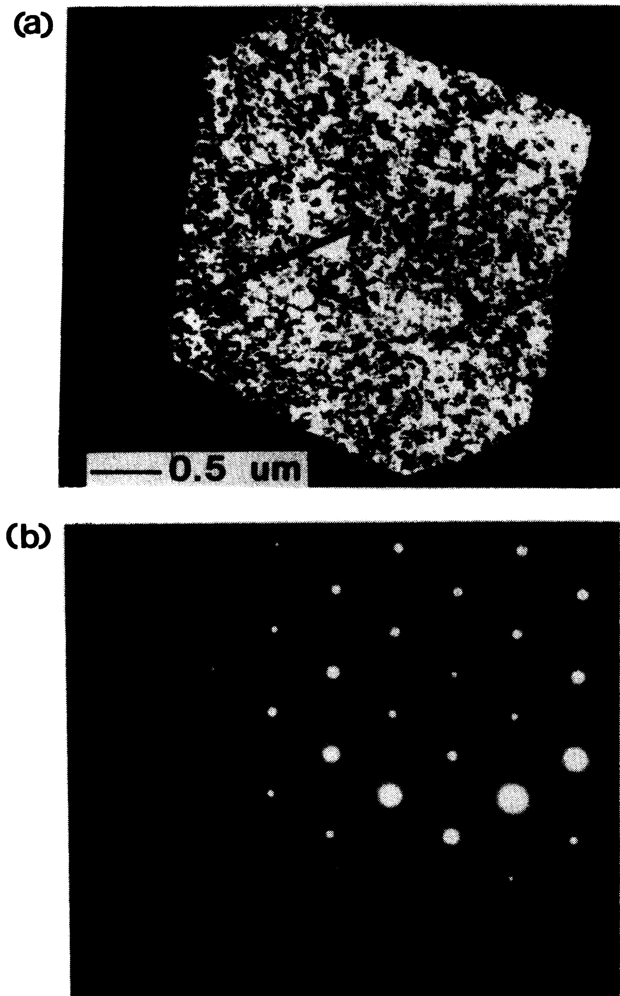

FIG. 8. (a) TEM planar micrograph and (b) diffraction pattern of the (110) pole of the crystal oriented within 12° from the normal of the sample surface. Au(150 nm)/polysilicon(400 nm) sample after *in situ* anneal in TEM.

saturation of Si in the Au, we do not think nucleation of Si grains plays a significant role in this reaction for two reasons. First of all, it does not seem reasonable from energy considerations that a nucleated Si crystal could grow faster than the much larger Si grains that already exist. The second reason deals with the orientation of the growing crystals. If the reaction proceeds with only grain growth and negligible nucleation, then the orientation of the initial set of grains would be the same as the final set of large grains. This is what was observed experimentally with the XRD pole-figure data. The distribution and orientation of the (110) poles of the as-deposited sample were the same as the annealed large-grained sample.

To further investigate the orientation relationship between the growing crystal and the substrate on which it grows, another experiment was performed.[22] A special sample was made for this experiment. Starting with the same polysilicon/SiO_2/Si substrate, the polysilicon and SiO_2 layer were removed (etched) from half of the sample, which exposes the (100) Si wafer on the other half of the sample. Au was then deposited over the entire wafer, allowing for a continuous Au film to laterally connect the

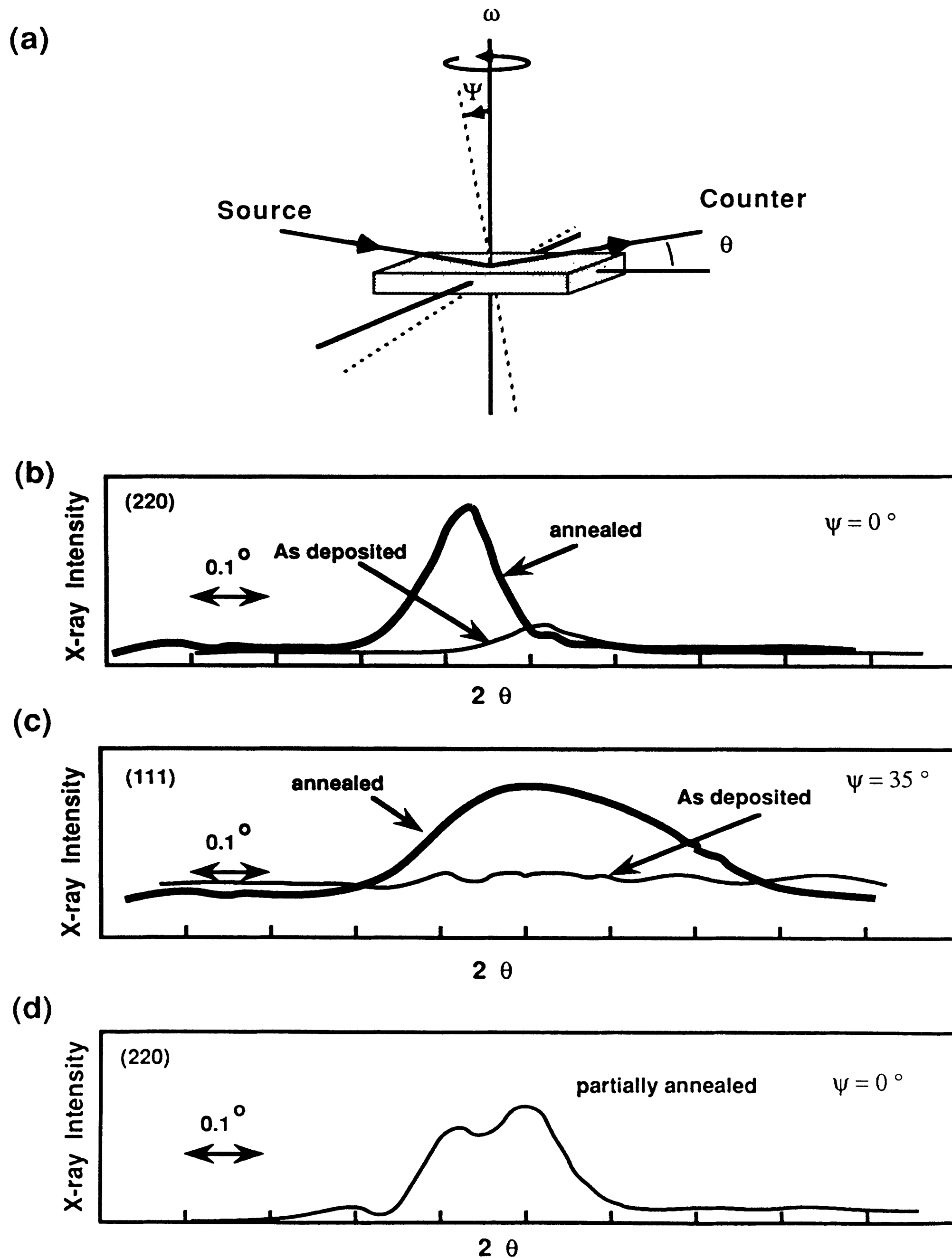

FIG. 9. XRD data of annealed and as-deposited samples (a) near the (220) peak with sample at $\psi=0°$, (b) near the (111) peak with $\psi=35°$, and a partially annealed sample at $\psi=0°$. Data indicate shift in peak position.

polysilicon side of the sample with the single-crystal (100) wafer side of the sample. During thermal annealing of this sample, Si was transported laterally (via the Au layer) from the polysilicon side to form individual Si crystals on the Si(100) side of the sample. These crystals are in the shape of right-angle prisms, which is the form expected of a growing (100) Si crystal, where the (111) prism faces are the slowest-growing sides of the crystal. All these crystals have the same physical orientation with respect to the substrate.

In both cases (Au/polysilicon or Au/single crystal Si) the orientation of the growing crystals emulates the orientation of the crystal at the surface it grows on. We deduce from these data that the origin of these crystals is due to the growth of already existing grains at the initial Au/Si interface and that nucleation is not significant.

A description of the overall process of the formation of the large-grained Si crystals in the Au/polysilicon is now suggested. After Au deposition the top-surface Si crystals begin to interact with each other. The Au layer acts as a short-circuit diffusion path for the Si. The average Si concentration in the Au will be below the solubility limit for the small grains (large curvature), so they will begin to dissolve, but Si concentration will be beyond the solubility limit for the large grains (small curvature) and they will begin to grow. The sequence for the growth process is illustrated in Fig. 10. Initially, the already existing large grains grow upward from the interface in a three-dimensional (3D) manner until they impinge on the top Au surface, and then they grow in a 2D manner radially to form two-dimensional platelike crystals. The growing Si crystals displaces the Au. Competition between the large grains will determine the final number or size of the grains. This topic will be investigated in the kinetic section of this study.[18]

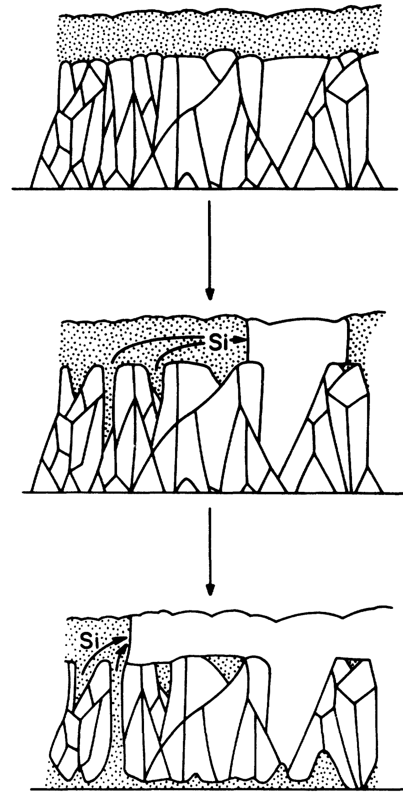

FIG. 10. Stages of grain growth of Si crystals. The initial structure is a bilayer of Au (top) and of polysilicon with various grain sizes (bottom). Note that the resultant large-grained crystal has the same orientation as the initial grain.

V. CONCLUSIONS

We have observed and analyzed the interaction between bilayers of Au and polycrystalline Si. The grain size of the Si can increase by a factor of 10 000 from the fine-grained polycrystalline Si to large two-dimensional single crystals upon thermal annealing at temperatures between 200 and 300 °C. The large crystals have the same (110) preferred orientation as the fine-grained polycrystalline Si.

Ostwald ripening (grain coarsening) is the basic process responsible for the formation of the crystals. Large grains of the initial polycrystalline Si film grow at the expense of the small grains. The Au film provides a fast-diffusion path for Si transport. Si from small grains dissolves into the Au layer, and then diffuses to the large crystal, which may be several microstructures away. The Au/polysilicon bilayer configuration allows for a unique two-dimensional growth process to occur, which gives rise to the possibility of growing arbitrarily shaped, two-dimensional, nonflat Si crystals.

The driving force for this small-grain–to–large-grain transformation is attributed to be the reduction of the free energy associated with the interface energy at the polysilicon grain boundaries. The origin of the crystals is concluded not to be nucleation, but rather the growth of already existing large grains (small curvature) initially at the Au/polysilicon interface.

ACKNOWLEDGMENTS

This work was supported in part by Cornell Microscience Center of the Semiconductor Research Corporation and IBM, General Technologies Division, (D. Campbell and E. Colgan), Hopewell Junction, NY. The authors wish to thank the staff and administrators at the National Nanofabrication Facility at Cornell University for the access to their thin-film-fabrication equipment. We thank the staff of the Material Science & Engineering (MS&E) microscopy facility, especially J. Hunt for the use and instruction of their (TEM and SEM) equipment and the Material Science and Engineering (MS&E) Geology XRD group, especially M. Rich and M. Weathers for their cooperation.

[1]L. Csepregi, E. F. Kennedy, and J. W. Mayer, J. Appl. Phys. **49**, 3906 (1978).

[2]H. Yamamoto, H. Ishiwara, S. Furukawa, M. Tamura, and T. Tokuyama, in *Thin Films and Interfaces II,* Vol. 25 of *Materials Research Society Symposium Proceedings,* edited by J. E. E. Baglin, D. R. Campbell, and W. K. Chu (MRS, Pittsburgh, 1984), p. 511.

[3]M. Moniwa, K. Kusukawa, E. Murakami, T. Warabisako, and M. Miyao, Appl. Phys. Lett. **52**, 1788 (1988).

[4]S. S. Lau and W. F. van der Weg, in *Thin Films—Interdiffusion and Reactions,* edited by J. M. Poate, K. N. Tu, and J. W. Mayer (Wiley, New York, 1978), Chap. 12.

[5]S. S. Lau *et al.*, in *Handbook on Semiconductors: Materials, Properties and Preparation,* edited by S. P. Keller (North-Holland, New York, 1980), Vol. 3, Chap. 8.

[6]J. O. McCaldin, J. Vac. Sci. Technol. **11**, 990 (1974).

[7]G. Ottaviani, D. Sigurd, V. Marrello, J. W. Mayer, and J. O. McCaldin, J. Appl. Phys. **45**, 1730 (1974).

[8]D. Sigurd, G. Ottaviani, H. J. Arnal, and J. W. Mayer, J. Appl. Phys. **45**, 1740 (1974).

[9]G. Ottaviani, K. N. Tu, and C. Nobili, in *Polysilicon Films and Interfaces, Materials Research Society Symposium Proceedings,* edited by C. Y. Wong, C. V. Thompson, and K. N. Tu (MRS, Pittsburgh, in press).

[10]K. Nakamura, M-A. Nicolet, and J. W. Mayer, J. Appl. Phys. **46**, 4678 (1975).

[11]K. Nakamura, J. O. Olowolafe, S. S. Lau, M-A. Nicolet, J. W. Mayer, and R. Shima J. Appl. Phys. **47**, 1278 (1976).

[12]K. Nakamura and M. Kamoshida, J. Appl. Phys. **48**, 5349 (1977).

[13]G. Majni and G. Ottaviani, Appl. Phys. Lett. **31**, 125 (1977).

[14]G. Majni, G. Ottaviani, and R. Stuck, Thin Solids Films **55**, 235 (1978).

[15]G. Ottaviani and G. Majni, J. Appl. Phys. **50**, 6865 (1979).

[16]C. R. M Grovenor and D. A. Smith, in *Thin Films and Interfaces II,* Vol. 25 of *Materials Research Society Symposium Proceedings,* edited by J. E. E. Baglin, D. R. Campbell, and W. K. Chu (MRS, Pittsburgh, 1984), p. 305.

[17]S. R. Herd, P. Chaudhari, and M. H. Brodsky, J. Non-Cryst. Solids **7**, 309 (1972).

[18]L. H. Allen, K. N. Tu, L. C. Feldman, and J. W. Mayer, following paper, Phys. Rev. B **41**, 8213 (1990).

[19]T. Kamins, *Polycrystalline Silicon for Integrated Circuit Applications* (Kluwer, Boston, 1988).

[20]B. D. Cullity, *Elements of X-Ray Diffraction* (Addison-Wesley, Reading, MA, 1978).

[21]R. A. Swalin, *Thermodynamics of Solids* (Wiley, New York, 1972).

[22]L. H. Allen (unpublished work).

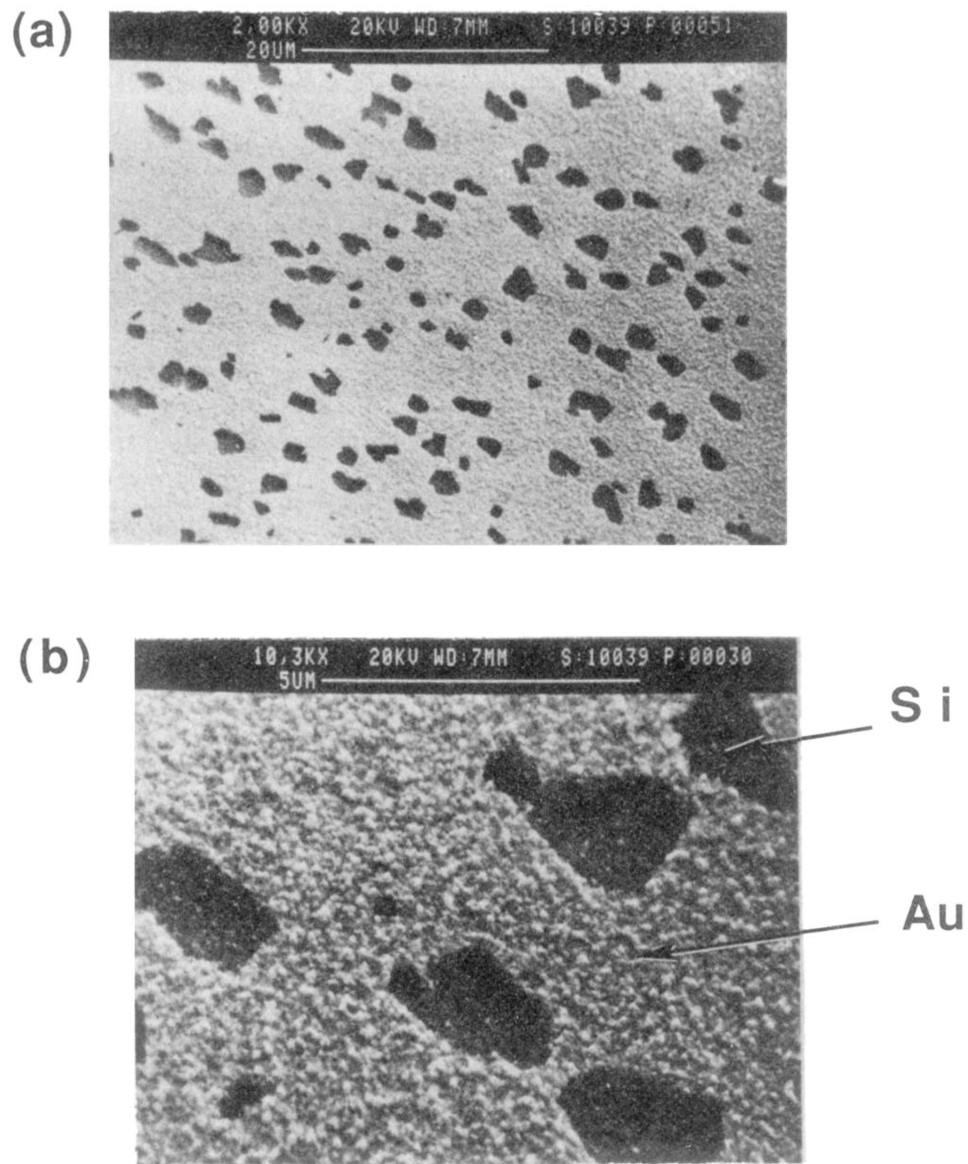

FIG. 1. SEM photograph of Au($\approx$ 170 nm)/polysilicon($\approx$ 400 nm)/SiO_2 after 270-°C vacuum-furnace annealing for 240 min.

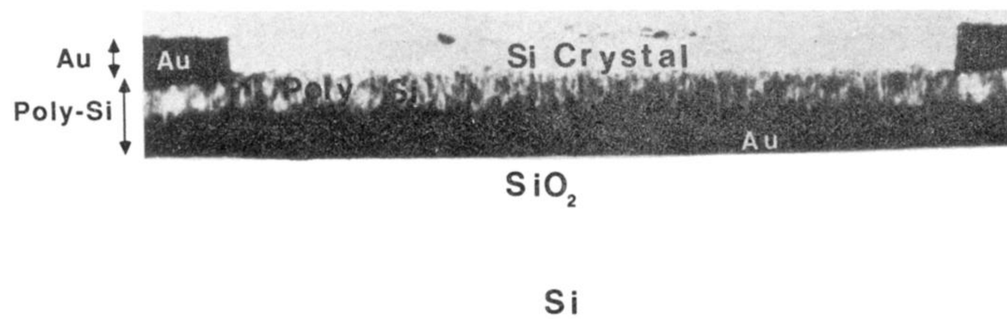

FIG. 2. Cross-sectional TEM data of Au($\approx$200 nm)/polysilicon($\approx$400 nm)/SiO_2 sample after 250-°C vacuum-furnace annealing.

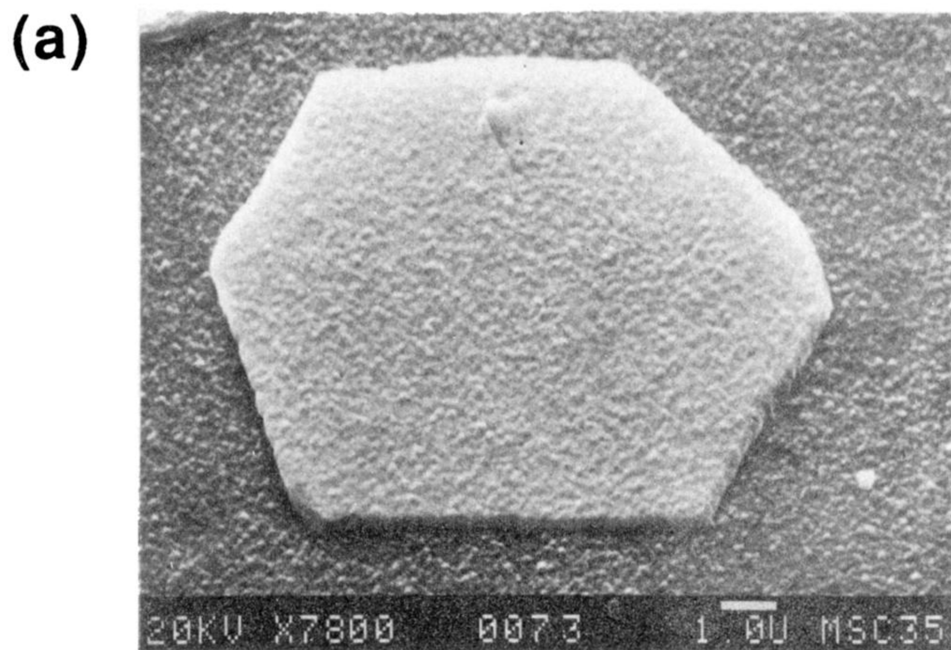

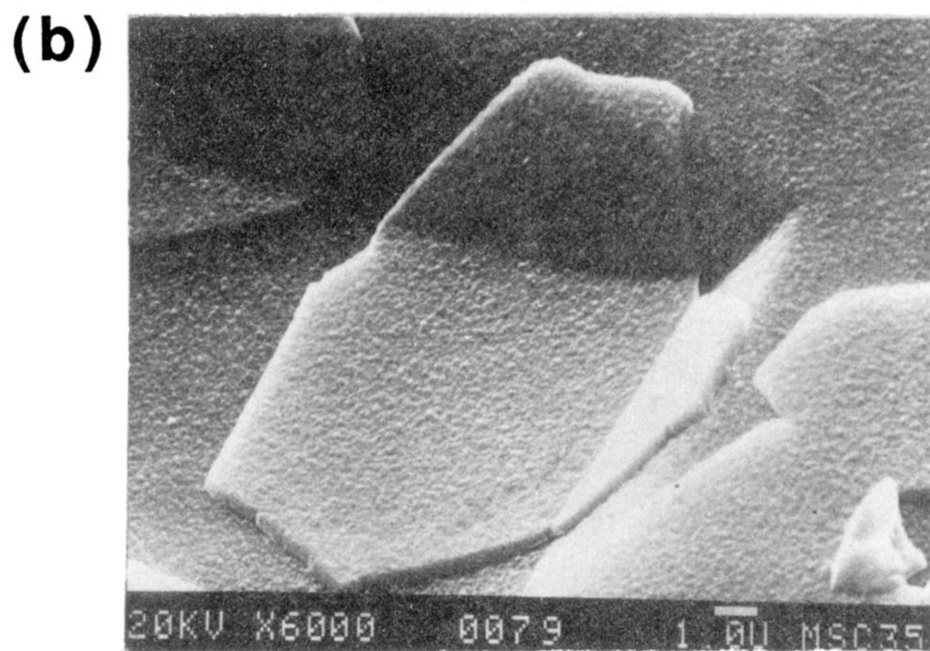

FIG. 3. SEM micrograph of Si crystals on polysilicon after Au was selectively etched. Au(≈ 250 nm)/polysilicon(≈ 400 nm)/SiO_2 samples were fabricated on (a) flat and (b) stepped-surface substrates.

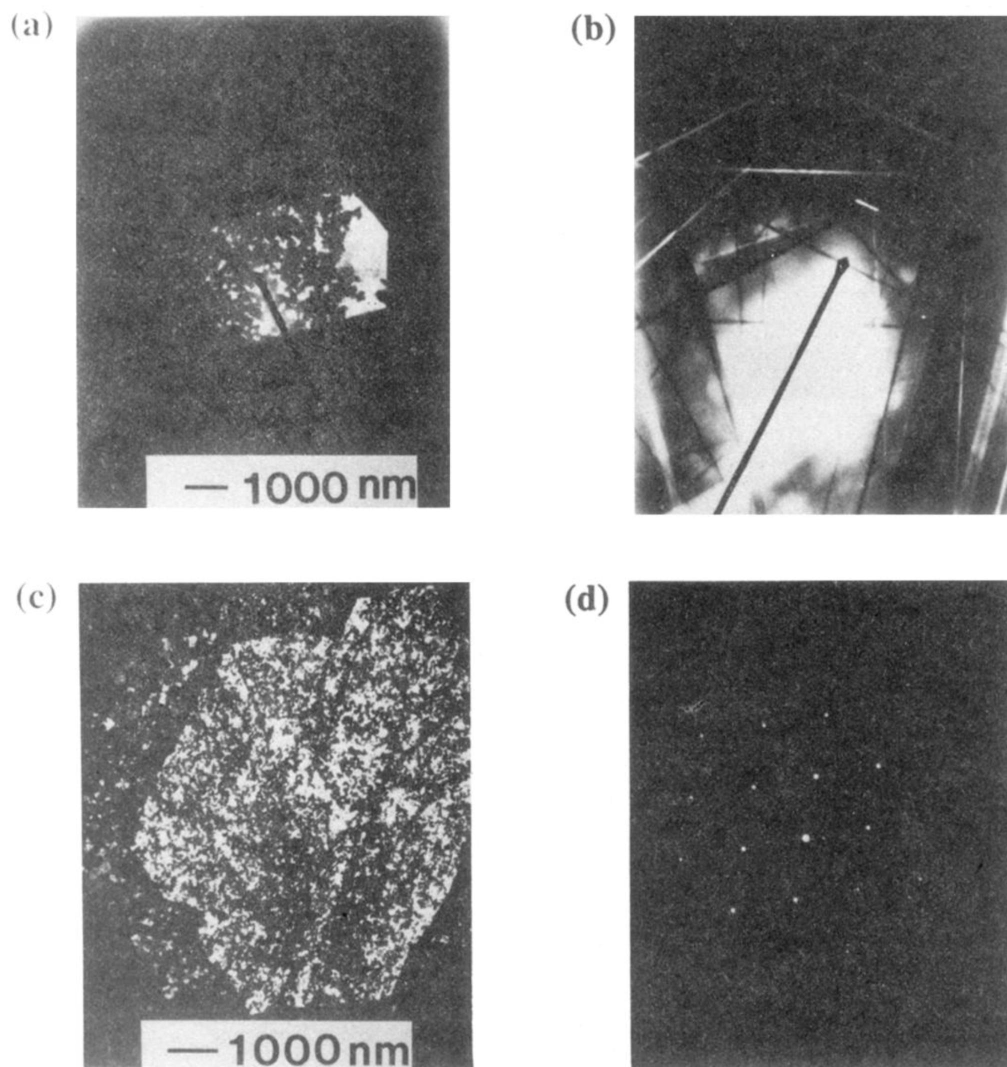

FIG. 4. BF image and diffraction micrographs of (a) and (b) thick and (c) and (d) thin Si crystals. The samples were made with thick [(a) and (b)] (200 nm) and thin [(c) and (d)] layers of Au on Si(100 nm). The Au/polysilicon samples were annealed (250–300 °C) *in situ* in TEM.

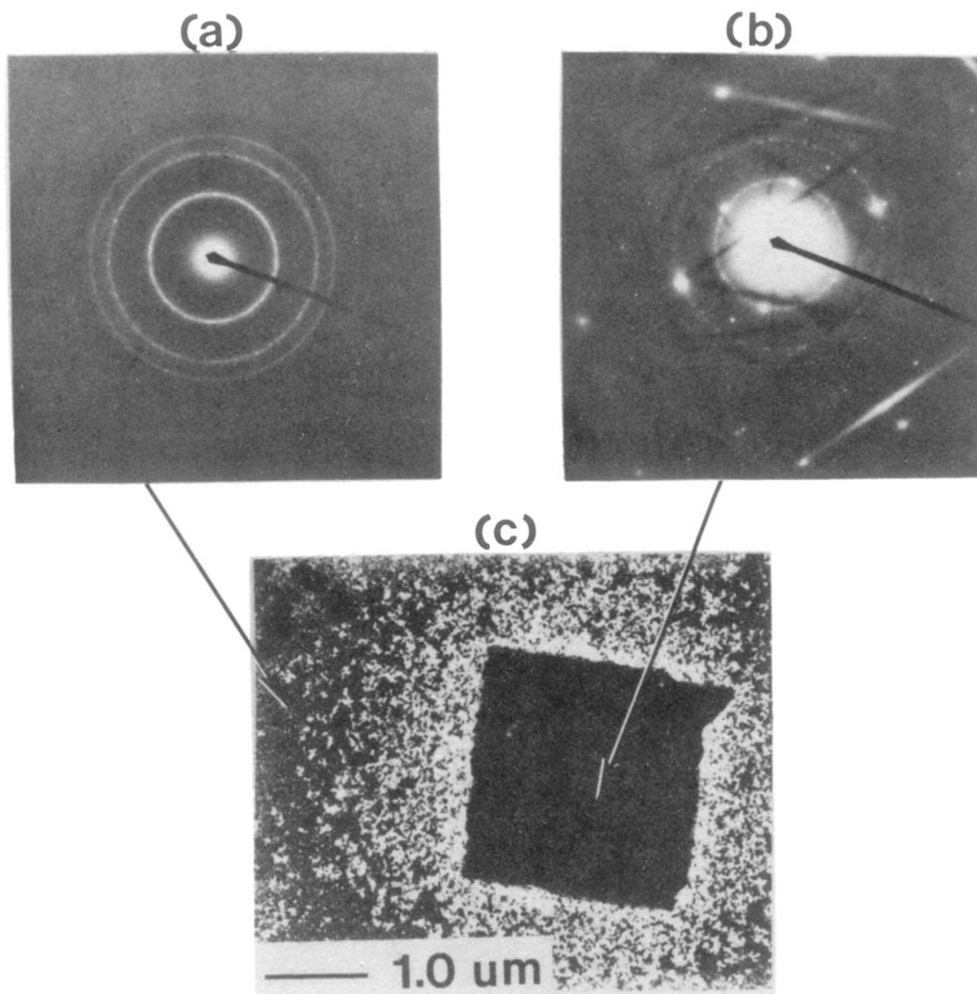

FIG. 5. Planar TEM data of Au(200 nm)/polysilicon(100 nm) *in situ* annealed sample after Au was etched, showing Si depletion in area adjacent to crystal: (a) Debye rings from the polysilicon, and (b) Kikuchi pattern and Debye rings from the crystal and polysilicon, and BF micrograph.

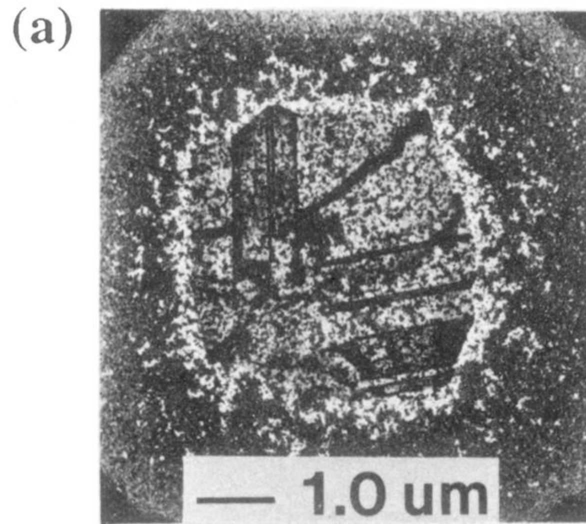

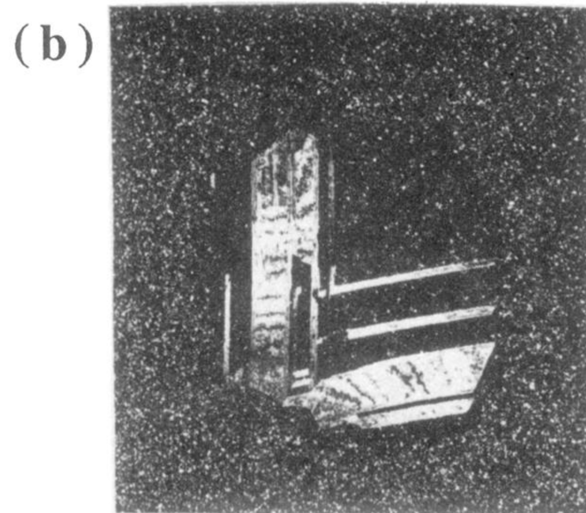

FIG. 6. (a) BF and (b) DF TEM micrographs of Si and polysilicon after Au selective etch. The Au(≈ 100 nm)/polysilicon(≈ 100 nm) samples were annealed *in situ* with TEM.

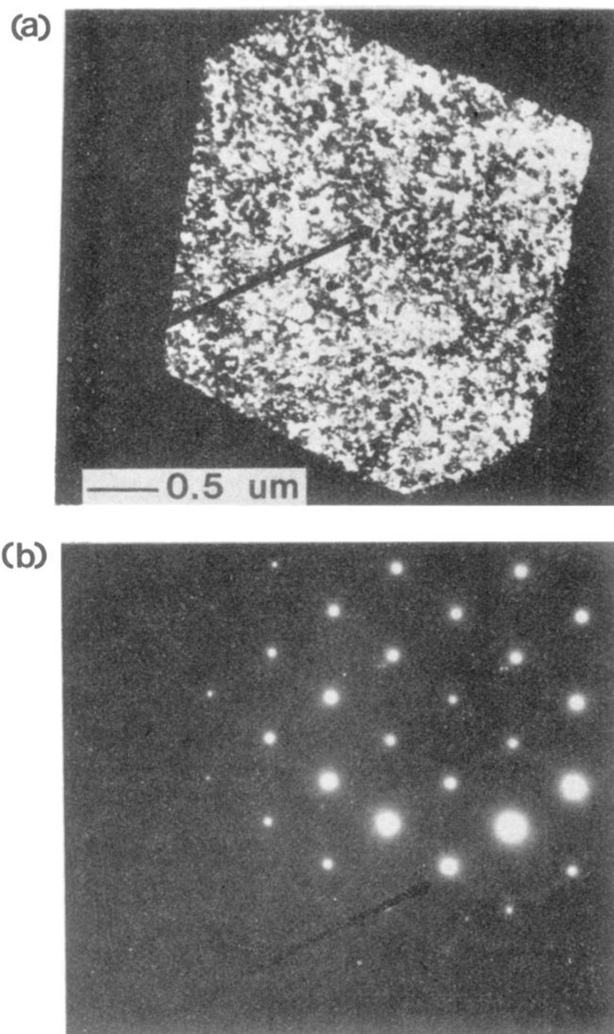

FIG. 8. (a) TEM planar micrograph and (b) diffraction pattern of the (110) pole of the crystal oriented within 12° from the normal of the sample surface. Au(150 nm)/polysilicon(400 nm) sample after *in situ* anneal in TEM.

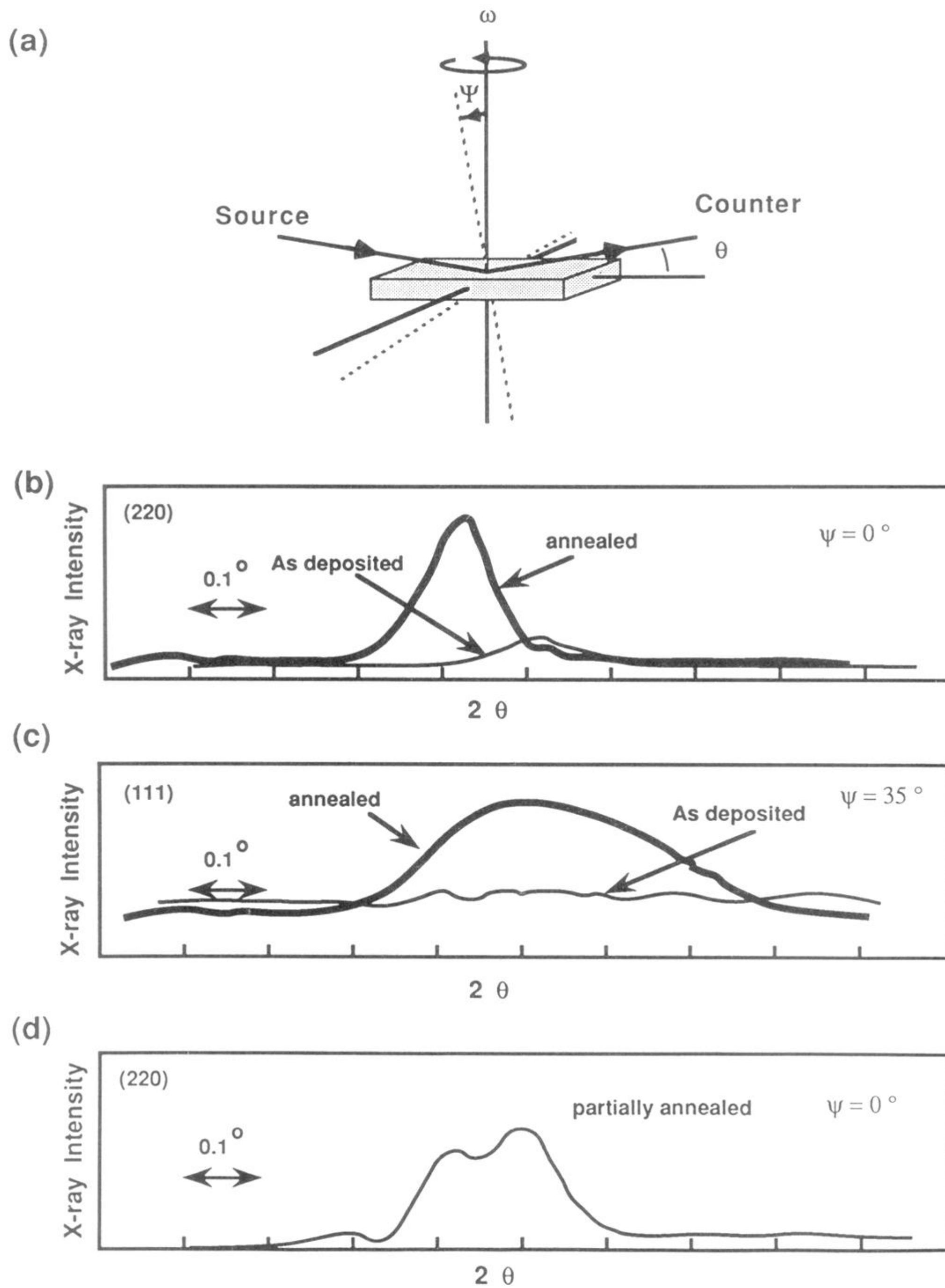

FIG. 9. XRD data of annealed and as-deposited samples (a) near the (220) peak with sample at $\psi = 0°$, (b) near the (111) peak with $\psi = 35°$, and a partially annealed sample at $\psi = 0°$. Data indicate shift in peak position.